Ultralong Dephasing Times in Solid-State Spin Ensembles via Quantum Control

Erik Bauch,[1,*] Connor A. Hart,[1,*] Jennifer M. Schloss,[1,2,3] Matthew J. Turner,[1,3] John F. Barry,[1,4] Pauli Kehayias,[1,5] Swati Singh,[6] and Ronald L. Walsworth[1,3,5,†]

[1]*Department of Physics, Harvard University, Cambridge, Massachusetts 02138, USA*
[2]*Department of Physics, Massachusetts Institute of Technology, Cambridge, Massachusetts 02139, USA*
[3]*Center for Brain Science, Harvard University, Cambridge, Massachusetts 02138, USA*
[4]*Lincoln Laboratory, Massachusetts Institute of Technology, Lexington, Massachusetts 02420, USA*
[5]*Harvard-Smithsonian Center for Astrophysics, Cambridge, Massachusetts 02138, USA*
[6]*Williams College, Department of Physics, 33 Lab Campus Drive, Williamstown, Massachusetts 01267, USA*

(Received 7 February 2018; revised manuscript received 4 June 2018; published 25 July 2018)

Quantum spin dephasing is caused by inhomogeneous coupling to the environment, with resulting limits to the measurement time and precision of spin-based sensors. The effects of spin dephasing can be especially pernicious for dense ensembles of electronic spins in the solid state, such as nitrogen-vacancy (NV) color centers in diamond. We report the use of two complementary techniques, spin-bath driving, and double quantum coherence magnetometry, to enhance the inhomogeneous spin dephasing time (T_2^*) for NV ensembles by more than an order of magnitude. In combination, these quantum control techniques (i) eliminate the effects of the dominant NV spin ensemble dephasing mechanisms, including crystal strain gradients and dipolar interactions with paramagnetic bath spins, and (ii) increase the effective NV gyromagnetic ratio by a factor of two. Applied independently, spin-bath driving and double quantum coherence magnetometry elucidate the sources of spin ensemble dephasing over a wide range of NV and bath spin concentrations. These results demonstrate the longest reported T_2^* in a solid-state electronic spin ensemble at room temperature and outline a path towards NV-diamond dc magnetometers with broadband femtotesla sensitivity.

DOI: 10.1103/PhysRevX.8.031025 Subject Areas: Magnetism, Quantum Physics

I. INTRODUCTION

Solid-state electronic spins, including defects in silicon carbide [1–5], phosphorus spins in silicon [6,7], and silicon-vacancy [3,8,9] and nitrogen-vacancy (NV) centers [10] in diamond, have garnered increasing relevance for quantum science and sensing experiments. In particular, NV centers in diamond have been extensively studied and deployed in diverse applications facilitated by long NV spin coherence times [11,12] at ambient temperature, as well as optical preparation and readout of NV spin states [10]. Many applications utilize dense NV spin ensembles for high-sensitivity dc magnetic-field sensing [13,14] and wide-field dc magnetic imaging [15–19], including measurements of single-neuron action potentials [13], paleomagnetism [19,20], and current flow in graphene [18].

For NV ensembles, the dc magnetic-field sensitivity is typically limited by dephasing of the NV sensor spins. In such instances, spin interactions with an inhomogeneous environment [see Fig. 1(a)] limit the experimental sensing time to the spin dephasing time $T_2^* \lesssim 1\ \mu$s [21–24]. Hahn echo and dynamical decoupling protocols can restore the NV ensemble phase coherence by isolating the NV sensor spins from environmental noise and, in principle, permit sensing times approaching the spin lattice relaxation ($T_1 \sim$ ms) [25–27]. However, these protocols restrict sensing to ac signals within a narrow bandwidth. For this reason, the development of high-sensitivity, broadband magnetometers requires new approaches to extend T_2^* for NV ensembles while retaining the ability to measure dc signals.

To date, spin dephasing mechanisms for NV ensembles have not been systematically studied, as spatially inhomogeneous effects do not lead to single NV spin dephasing, which has traditionally been the focus of the NV-diamond literature [11,29–31]. Here, we characterize and control the dominant NV spin ensemble dephasing mechanisms by combining two quantum control techniques, double quantum (DQ) coherence magnetometry [30,31] and spin-bath driving [32,33]. We apply these techniques to three isotopically engineered ^{12}C samples with widely varying

*E. B. and C. A. H. contributed equally to this work.
†rwalsworth@cfa.harvard.edu

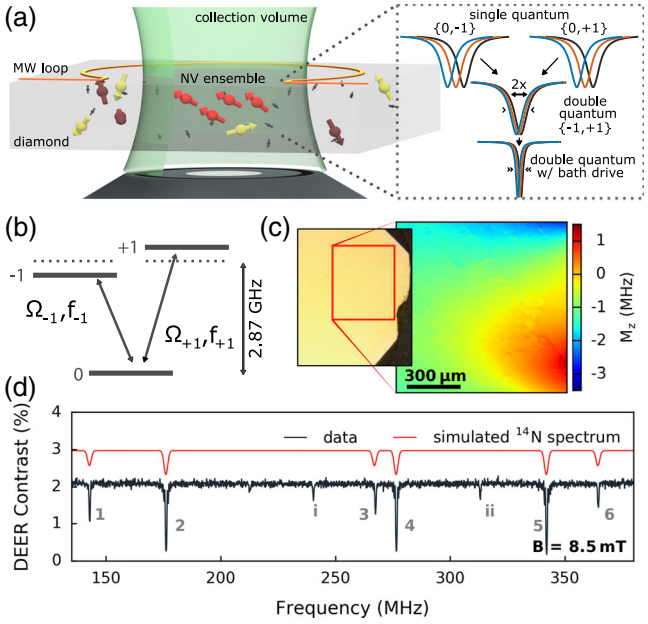

FIG. 1. NV ensemble spectroscopy of diamond spin bath. (a) The inhomogeneously broadened electron spin resonance (ESR) linewidth of NV ensembles is a complex function of the local environment within the diamond sample, which includes a diverse bath of electronic and nuclear spins. Inset: Schematics of NV ensemble ESR spectra in the single quantum and double quantum bases, and for double quantum with spin-bath drive. (b) Spin-1 ground state of the NV center. (c) Imaging of the longitudinal strain component M_z of one NV orientation class across a 1-mm^2 field of view for sample B. An optical microscope image of the diamond surface (left) is included for reference with a red box outlining the field of view shown in the NV strain image. (d) NV double electron-electron resonance (DEER) spectrum of sample B, showing six nitrogen groups (1–6) attributed to ^{14}N electronic spins with an external field $B_0 =$ 8.5 mT aligned along a [111]-crystallographic axis (see main text). Linewidths are Fourier broadened. The peaks labeled *i* and *ii* correspond to dipole-forbidden transitions of the ^{14}N electronic spins ($\Delta m_I \neq 0$; see Supplemental Material Sec. XI [28]). The simulated spectrum using the full nitrogen Hamiltonian is shown in red, with linewidth and amplitudes chosen to reflect the experimental data.

nitrogen and NV concentrations. In combination, we show that these quantum control techniques can extend the NV spin ensemble T_2^* by more than an order of magnitude.

Several inhomogeneous spectral broadening mechanisms can contribute to NV spin ensemble dephasing in bulk diamond. First, the formation of negatively charged NV^- centers (with electronic spin $S = 1$) requires the incorporation of nitrogen into the diamond lattice. As a result, paramagnetic substitutional nitrogen impurities (P1 centers, $S = 1/2$) [34–36] typically persist at densities similar to or exceeding the NV concentration, leading to a "spin bath" that couples to the NV spins via incoherent dipolar interactions, with a magnitude that can vary significantly across the NV ensemble. Second, ^{13}C nuclei ($I = 1/2$) can be a considerable source of NV spin dephasing in diamonds with natural isotopic abundance (1.07%), with the magnitude of this effect varying spatially due to the random location of ^{13}C within the diamond lattice [37,38]. Such NV spin ensemble dephasing, however, can be greatly reduced through isotope engineering of the host diamond material [11]. Third, strain is well known to affect the diamond crystal and the zero-magnetic-field splitting between NV spin states [39,40]. The exact contribution of strain gradients to NV spin ensemble dephasing has not been quantified rigorously because strain varies throughout and between samples, and it is, in part, dependent upon the substrate used for diamond growth [41,42]. Furthermore, the interrogation of spatially large NV ensembles requires the design of uniform magnetic bias fields to minimize magnetic-field gradients across the detection volume.

We assume that the relevant NV spin ensemble dephasing mechanisms are independent and can be summarized by Eq. (1),

$$\frac{1}{T_2^*} \approx \frac{1}{T_2^*\{\text{NV-}^{13}\text{C}\}} + \frac{1}{T_2^*\{\text{NV-N}\}} + \frac{1}{T_2^*\{\text{other spins}\}} + \frac{1}{T_2^*\{\text{strain grad.}\}} + \frac{1}{T_2^*\{\text{B-field grad.}\}} + \frac{1}{T_2^*\{\text{temp. fluctuations}\}} + \cdots, \quad (1)$$

where $T_2^*\{\cdot\}$ describes the T_2^* limit imposed by a particular dephasing mechanism, and the "≈" symbol indicates that individual dephasing rates add approximately linearly.

DQ magnetometry employs the $\{-1, +1\}$ sub-basis of the NV spin-1 system for quantum sensing. In this basis, noise sources that shift the $|\pm 1\rangle$ states in common mode [e.g., strain inhomogeneities and spectrum drifts due to temperature fluctuations of the host diamond; the fourth and sixth term in Eq. (1), respectively] are suppressed by probing the energy difference between the $|+1\rangle$ and $|-1\rangle$ spin states. In addition, the NV DQ spin coherence accumulates phase due to an external magnetic field at twice the rate of traditional single quantum (SQ) coherence magnetometry, for which the $|0\rangle$ and $|+1\rangle$ (or $|-1\rangle$) spin states are probed. DQ magnetometry provides enhanced susceptibility to target magnetic-field signals while also making the spin coherence twice as sensitive to magnetic noise, including interactions with the paramagnetic spin bath. We, therefore, use resonant radio-frequency control to decouple the bath spins from the NV sensors [the second and third terms in Eq. (1)]. By employing both DQ magnetometry and spin-bath driving with isotopically enriched samples, we elucidate and effectively eliminate the dominant sources of NV spin ensemble dephasing, realizing up to a 16× extension of the ensemble T_2^* in diamond. These techniques are also compatible with

Ramsey-based dc sensing, and we find up to an 8× improvement in dc magnetic-field sensitivity. Our results should enable broadband dc sensing using NV spin ensembles with spin interrogation times approaching those used in ac sensing and may aid in the fabrication of optimized samples for a wide range of solid-state sensor species.

A. Double quantum magnetometry

The enhanced sensitivity to magnetic fields and insensitivity to common-mode noise sources in this DQ basis can be understood by considering the full ground-state Hamiltonian for NV centers, given by (neglecting the hyperfine interaction) [10]

$$H/h = DS_z^2 + \frac{\gamma_{\mathrm{NV}}}{2\pi}\mathbf{B}\cdot\mathbf{S} + M_z S_z^2 + M_x(S_y^2 - S_x^2) + M_y(S_x S_y + S_y S_x), \quad (2)$$

where $D \approx 2.87$ GHz is the zero-field spin-state splitting; $\mathbf{S} = \{S_x, S_y, S_z\}$ are the dimensionless spin-1 operators; $\mathbf{B} = \{B_x, B_y, B_z\}$ are the local magnetic-field components; $\gamma_{\mathrm{NV}}/2\pi \approx 28$ GHz/T is the NV gyromagnetic ratio; and $\{M_x, M_y, M_z\}$ describe the strain and electric field contributions to H [43]. Ignoring terms $\propto S_x$, S_y due to the large zero-field splitting D and a small applied bias $B_z \gtrsim 10$ mT along z, the transition frequencies $f_{\pm1}$ [see Fig. 1(b)] are

$$f_{\pm1} \approx D + M_z \pm \frac{\gamma_{\mathrm{NV}}}{2\pi}B_z. \quad (3)$$

On-axis strain contributions ($\propto M_z$), as well as temperature fluctuations ($\partial D/\partial T = -74$ kHz/K) [21,44], shift the $f_{\pm1}$ transitions linearly. Thus, when performing DQ magnetometry where the difference $\Delta f = f_{+1} - f_{-1}$ is probed, their effects are to first order suppressed. In addition, a perturbative analysis of the complete Hamiltonian in Eq. (2) (see Supplemental Material Sec. VII [28]) shows that the effects of off-axis strain contributions ($\propto M_x$, M_y) on DQ magnetometry are reduced by a factor $\sqrt{M_x^2 + M_y^2}/(\gamma_{\mathrm{NV}}B_z/\pi)$, proportional to the bias magnetic field B_z. Similarly, the effects of off-axis magnetic fields ($\propto B_x$, B_y) on DQ magnetometry are suppressed due to the large zero-field splitting D, and they are also largely common mode. Working in the DQ basis at moderate bias fields can, therefore, lead to an enhancement in T_2^* for NV ensembles if strain inhomogeneities; small off-axis magnetic-field gradients (B_x, $B_y \ll D$); or temperature fluctuations are significant mechanisms of inhomogeneous spin dephasing. This result should be contrasted with single NV measurements in which T_2^* and T_2 in the DQ basis were found to be approximately half the values in the SQ basis, i.e., $\tau_{\mathrm{DQ}}^{\mathrm{coh}} \approx \tau_{\mathrm{SQ}}^{\mathrm{coh}}/2$ [30,31]. Since spatial inhomogeneities are not relevant for single centers, the reduced decay times are attributed to an increased sensitivity to magnetic noise in the DQ basis due to the paramagnetic spin bath.

For example, using vector magnetic microscopy (VMM) [19], we mapped the on-axis strain component M_z in a 1-mm^2 region for one of the three NV ensemble diamond samples studied in this work ([N] = 0.75 ppm, sample B) to quantify the length scale and magnitude of strain inhomogeneity [Fig. 1(c)]. From this analysis, we estimate an average strain gradient $M_z/L \approx 2.8$ kHz/μm, which, as we show below, is in good agreement with the observed SQ T_2^* in our samples.

B. Spin-bath driving

To mitigate NV spin dephasing due to the spin bath, we drive the bath electronic spins [32,33] using resonant radio-frequency (rf) radiation. In Fig. 1(d), we display the spin resonance spectrum of a nitrogen-rich diamond sample ([N] = 0.75 ppm, sample B), recorded via the NV DEER technique [45] in the frequency range 100–500 MHz (see Supplemental Material Sec. IX [28]). The data reveal six distinct spectral peaks attributed to ^{14}N substitutional defects in the diamond lattice. The resonance peaks have an approximate amplitude ratio of 1:3:1:3:3:1, resulting from the four crystallographic Jahn-Teller orientations of the nitrogen defects at two possible angles with respect to an applied bias magnetic field ($B_z = 8.5$ mT, aligned along the [111]-axis), as well as three hyperfine states [46–48] (see Supplemental Material Sec. IX [28] for details). Additional smaller peaks i and ii are attributed to dipole-forbidden nitrogen spin transitions and other electronic dark spins [49].

In pulsed spin-bath driving [32], a multifrequency rf π-pulse is applied to each of the bath spin resonances midway through the NV Ramsey sequence, decoupling the bath from the NV sensor spins in analogy to a refocusing π-pulse in a spin echo sequence [25]. Alternatively, the bath spins can be driven with continuous wave (cw) [32,33]. In this case, the Rabi drive strength Ω_{Bath} at each bath spin resonance frequency must significantly exceed the characteristic coupling strength γ between the bath spins and NV centers, i.e., $\Omega_{\mathrm{Bath}}/\gamma \gg 1$, to achieve effective decoupling. Under this condition, the bath spins undergo many Rabi oscillations during the characteristic dipolar interaction time $1/\gamma$. As a result, the dipolar interaction with the bath is incoherently averaged and the NV spin dephasing time increases.

II. RESULTS

We studied three diamond samples with increasing nitrogen concentrations that are summarized in Table I. Samples A ([N] $\lesssim 0.05$ ppm) and B ([N] = 0.75 ppm) each consist of a ^{14}N-doped, approximately 100-μm-thick chemical-vapor-deposition (CVD) layer (99.99% ^{12}C) deposited on top of a diamond substrate. Sample C ([N] = 10 ppm) possesses a 40-μm-thick, ^{15}N-doped CVD

TABLE I. Characteristics of samples A, B, and C. The estimated values $T_2^{*,\mathrm{est}}$ are calculated using the contributions of ^{13}C and nitrogen spins as described in the main text. Reasonable agreement is found between the estimated $T^{*,\mathrm{est}}_{2,\mathrm{NV}-(^{13}\mathrm{C+N})}$ and twice the measured $T^{*,\mathrm{meas}}_{2,\mathrm{DQ}}$, consistent with the twice faster dephasing in the DQ basis. Values listed with a $\sim$ symbol are order-of-magnitude estimates. For all samples, [NV] $\ll$ [N] and NV contributions to T_2^* can be neglected (1 ppm $= 1.76 \times 10^{17}\mathrm{cm}^{-3}$).

Sample	[N] (ppm)	^{13}C (%)	[NV] (cm^{-3})	T_2^{meas} (μs)	$T^{*,\mathrm{meas}}_{2,\mathrm{SQ}}$ (μs)	$T^{*,\mathrm{meas}}_{2,\mathrm{DQ}}$ (μs)	$T^{*,\mathrm{est}}_{2,\mathrm{NV\text{-}N}}$ (μs)	$T^{*,\mathrm{est}}_{2,\mathrm{NV}-^{13}\mathrm{C}}$ (μs)	$T^{*,\mathrm{est}}_{2,\mathrm{NV}-(^{13}\mathrm{C+N})}$ (μs)	dM_z^{meas}/dL (MHz/μm)
A	$\lesssim$0.05	0.01	$\sim 3 \times 10^{12}$	$\gtrsim$630	5–12	34(2)	350	100	78	n/a
B	0.75	0.01	$\sim 10^{14}$	250–300	1–10	6.9(5)	23	100	19	0.0028
C	10	0.05	$\sim 6 \times 10^{15}$	15–18	0.3–1.2	0.60(2)	2	20	2	n/a

layer (99.95% ^{12}C) on a diamond substrate. For all three samples, the nitrogen-limited NV dephasing times can be estimated from the average dipolar interaction strength between electronic spins giving $T^*_{2,\mathrm{NV\text{-}N}} \approx 350$, 23, and 2 μs for samples A, B, and C, respectively. Analysis and measurements suggest that the ^{13}C nuclear spin-bath limit to T_2^* is approximately 100 μs for samples A and B and approximately 20 μs for sample C (for details, see Supplemental Material Sec. V [28]). All samples are unirradiated and the N-to-NV conversion efficiency is $\lesssim$1%. Contributions from NV-NV dipolar interactions to T_2^* can, therefore, be neglected. The parameter regime covered by samples A, B, and C was chosen to best illustrate the efficacy of DQ coherence magnetometry and spin-bath driving.

We measured T_2^* values in the SQ and DQ bases, denoted $T^*_{2,\mathrm{SQ}}$ and $T^*_{2,\mathrm{DQ}}$ from here on, by performing a single- or two-tone $\pi/2 - \tau - \pi/2$ Ramsey sequence, respectively (see the inset in Fig. 2). In both instances, the observed Ramsey signal exhibits a characteristic stretched exponential decay envelope that is modulated by the frequency detunings of the applied NV drive(s) from the NV hyperfine transitions. We fit the data to the expression $C_0 \exp\left[-(\tau/T_2^*)^p\right] \sum_i \cos[2\pi f_i(\tau - \tau_{0,i})]$, where the free parameters in the fit are the maximal contrast C_0 at $\tau = 0$, dephasing time T_2^*, stretched exponential parameter p, time offsets $\tau_{0,i}$, and (up to) three frequencies f_i from the NV hyperfine splittings. The p value provides a phenomenological description of the decay envelope, which depends on the specific noise sources in the spin bath, as well as the distribution of individual resonance lines within the NV ensemble. For a purely magnetic-noise-limited spin bath, the NV ensemble decay envelope exhibits simple exponential decay ($p = 1$) [50,51], whereas a noninteger p-value ($p \neq 1$) suggests magnetic and/or strain-gradient-limited NV spin ensemble dephasing.

A. Strain-dominated dephasing (Sample A: Low nitrogen density regime)

Experiments on sample A ([N] $\lesssim 0.05$ ppm, ^{14}N) probed the low nitrogen density regime. In different regions of this diamond, the measured SQ Ramsey dephasing time varies between $T^*_{2,\mathrm{SQ}} \simeq 5$ and 12 μs, with $1 < p < 2$. Strikingly, even the longest measured $T^*_{2,\mathrm{SQ}}$ is approximately 30× shorter than the calculated $T^*_{2,\mathrm{NV\text{-}N}}$ given by the nitrogen concentration of the sample ($\gtrsim 350$ μs; see Table I) and is approximately 10× smaller than the expected SQ limit due to 0.01% ^{13}C spins ($\simeq 100$ μs). This discrepancy indicates that dipolar broadening due to paramagnetic spins is not the dominant NV dephasing mechanism. Indeed, the spatial

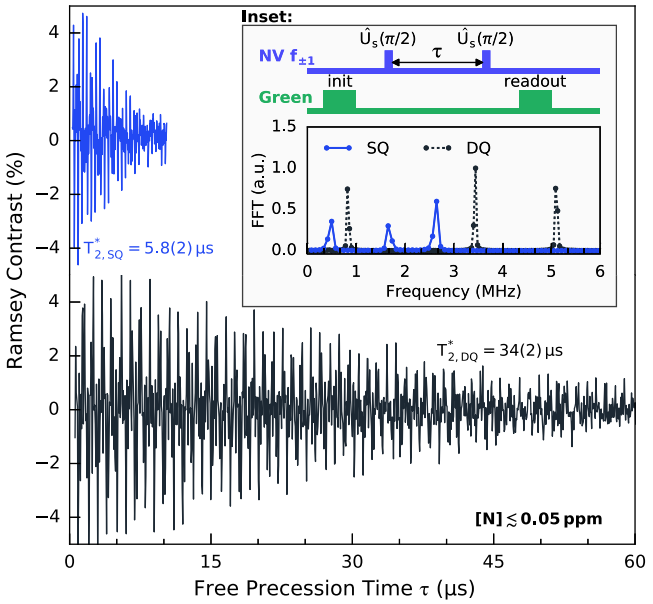

FIG. 2. NV Ramsey measurements for a low nitrogen density sample (sample A, [N] $\lesssim 0.05$ ppm) at an applied bias magnetic field of $B_0 = 2.2$ mT. Comparison of time-domain data and resulting fit values for the NV spin ensemble T_2^* for the single quantum (SQ) coherence, $\{0, +1\}$ (blue, upper) and the double quantum (DQ) coherence, $\{+1, -1\}$ (black, lower). Upper inset: Illustration of DQ Ramsey protocol with two-tone microwave (mw) pulses, where $\hat{U}_{S=1}(\pi/2)$ is the spin-1 unitary evolution operator [31]. For SQ measurements, a single-tone mw pulse is applied instead to generate the pseudo-spin-1/2 unitary evolution operator $\hat{U}_{S=1/2}(\pi/2)$. Lower inset: Discrete Fourier transform of the SQ (solid blue) and DQ (dashed black) Ramsey measurements with a mw drive detuned 0.4 MHz from the $\{0, \pm 1\}$ transitions. NV sensor spins accumulate phase twice as quickly in the DQ basis as in the SQ basis.

variation in $T^*_{2,SQ}$ and low concentration of nitrogen and ^{13}C spins suggest that crystal lattice strain inhomogeneity is the main source of NV spin ensemble dephasing in this sample. For the measured NV ensemble volume (approximately 10^4 μm^3) and the reference strain gradient [Fig. 1(c)], we estimate a strain-gradient-limited dephasing time of approximately 6 μs, in reasonable agreement with the observed $T^*_{2,SQ}$. Measurements in the DQ basis at moderate bias magnetic fields are to first order strain insensitive and, therefore, provide a means to eliminate the dominant contribution of strain to NV spin ensemble dephasing. Figure 2 shows data for T^*_2 in both the SQ and DQ bases for an example region of sample A with SQ dephasing time $T^*_{2,SQ} = 5.8(2)$ μs and $p = 1.7(2)$. For these measurements, we applied a small 2.2-mT bias field parallel to one NV axis (misalignment angle $< 3°$) to lift the $|\pm 1\rangle$ degeneracy, and we optimized the magnet geometry to reduce magnetic-field gradients over the sensing volume (see Supplemental Material Sec. VI [28]). In the DQ basis, we find $T^*_{2,DQ} = 34(2)$ μs with $p = 1.0(1)$, which is approximately a 6× improvement over the measured T^*_2 in the SQ basis. We observed similar T^*_2 improvements in the DQ basis in other regions of this diamond. Our results suggest that in the low nitrogen density regime, dipolar interactions with the ^{13}C nuclear spin bath are the primary decoherence mechanism when DQ basis measurements are employed to remove strain and temperature effects. Specifically, the measured $T^*_{2,DQ}$ and p values in sample A are consistent with the combined effect of NV dipolar interactions with (i) the 0.01% concentration of ^{13}C nuclear spins ($T^*_{2,N\text{-}^{13}C}/2 \simeq 50$ μs) and (ii) residual nitrogen spins $[N] \sim 0.05$ ppm, with an estimated net effect of $T^*_{2,DQ} \simeq 39$ μs. Diamond samples with greater isotopic purity ($^{12}C > 99.99\%$) would likely yield further enhancements in $T^*_{2,DQ}$.

B. Strain- and dipolar-dominated dephasing (Sample B: Intermediate nitrogen density regime)

Although sample B ($[N] = 0.75$ ppm, ^{14}N) contains more than an order of magnitude higher nitrogen spin concentration than sample A ($[N] \lesssim 0.05$ ppm), we observed SQ Ramsey dephasing times $T^*_{2,SQ} \simeq 1$–10 μs in different regions of sample B, which are similar to the results from sample A. We conclude that strain inhomogeneities are also a significant contributor to NV spin ensemble dephasing in sample B. Comparative measurements of T^*_2 in both the SQ and DQ bases yield a more moderate increase in $T^*_{2,DQ}$ for sample B than for sample A. Example Ramsey measurements of sample B are displayed in Fig. 3, showing $T^*_{2,SQ} = 1.80(6)$ μs in the SQ basis, increasing to $T^*_{2,DQ} = 6.9(5)$ μs in the DQ basis, approximately a 4× extension. The observed $T^*_{2,DQ}$ in sample B approaches the expected limit set by dipolar coupling of

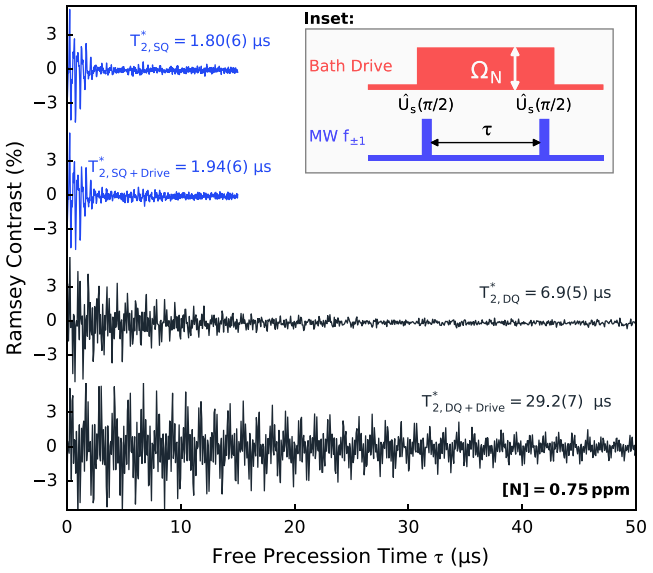

FIG. 3. NV Ramsey measurements for an intermediate nitrogen density sample (sample B, $[N] = 0.75$ ppm) at an applied bias magnetic field of $B_0 = 8.5$ mT. Comparison of time-domain data and resulting fit values for the NV spin ensemble T^*_2 for the SQ coherence $\{0, +1\}$ (blue, first from top); the SQ coherence with spin-bath drive (blue, second from top); the DQ coherence with no drive (black, third from top); and the DQ coherence with spin-bath drive (black, fourth from top). There is a 16.2× improvement of T^*_2 with spin-bath drive when the DQ coherence is used for sensing compared to SQ with no drive. Inset: Two-tone NV Ramsey protocol with an applied spin-bath drive resonant with nitrogen spins.

NV spins to residual nitrogen spins in the diamond ($T^*_{2,N\text{-}NV}/2 \simeq 12$ μs), but it is still well below the expected DQ limit due to 0.01% ^{13}C nuclear spins ($\simeq 50$ μs).

Measuring NV Ramsey decay in both the SQ and DQ bases while driving the nitrogen spins, either via application of cw or pulsed rf fields [32,33], is effective in revealing the electronic spin-bath contribution to NV ensemble dephasing. With continuous drive fields of Rabi frequency $\Omega_N = 2$ MHz applied to nitrogen spin resonances 1–6, i, and ii [see Fig. 1(d)], we find that $T^*_{2,SQ+Drive} = 1.94(6)$ μs, which only marginally exceeds $T^*_{2,SQ} = 1.80(6)$ μs. This result is consistent with NV ensemble SQ dephasing being dominated by strain gradients in sample B, rendering spin-bath driving ineffective in the SQ basis. In contrast, DQ Ramsey measurements exhibit a significant additional increase in T^*_2 when the bath drive is applied, improving from $T^*_{2,DQ} = 6.9(5)$ μs to $T^*_{2,DQ+Drive} = 29.2(7)$ μs. This approximately 16× improvement over $T^*_{2,SQ}$ confirms that, for sample B without spin-bath drive, dipolar interactions with the nitrogen spin bath are the dominant mechanism of NV spin ensemble dephasing in the DQ basis. Note that the NV dephasing time for sample B with DQ plus spin-bath drive is only slightly below that for

sample A with DQ alone (approximately 34 μs). We attribute this T_2^* limit in sample B primarily to NV dipolar interactions with 0.01% ^{13}C nuclear spins. There is also an additional small contribution from magnetic-field gradients over the detection volume (approximately 10^4 μm^3) due to the four times larger applied bias field ($B_0 = 8.5$ mT) relative to sample A, which was used in sample B to resolve the nitrogen ESR spectral features (see Supplemental Material Tables S3 and S4 [28]). We obtained similar extensions of T_2^* using pulsed driving of the nitrogen bath spins (see Supplemental Material Sec. X [28]).

We also characterized the efficacy of cw spin-bath driving for increasing T_2^* in both the SQ and DQ bases [see Fig. 4(a)]. While $T^*_{2,\mathrm{SQ}}$ remains approximately constant with varying Rabi drive frequency Ω_N, $T^*_{2,\mathrm{DQ}}$ exhibits an initial rapid increase and saturates at $T^*_{2,\mathrm{DQ}} \approx 27$ μs for $\Omega_\mathrm{N} \gtrsim 1$ MHz (only resonances 1–6 are driven here). To explain the observed trend, we introduce a model that distinguishes between (i) NV spin ensemble dephasing due to nitrogen bath spins, which depends upon bath drive strength Ω_N, and (ii) dephasing from drive-independent sources (including strain and ^{13}C spins),

$$1/T_2^* = 1/T^*_{2,\mathrm{NV\text{-}N}}(\Omega_\mathrm{N}) + 1/T^*_{2,\mathrm{other}}. \tag{4}$$

Taking the coherent dynamics of the bath drive into account (see Supplemental Material Sec. VIII [28]), the data are well described by the functional form

$$1/T^*_{2,\mathrm{NV\text{-}N}}(\Omega_\mathrm{N}) = \Delta m \times \gamma_{\mathrm{NV\text{-}N}} \frac{\delta_\mathrm{N}^2}{\delta_\mathrm{N}^2 + \Omega_\mathrm{N}^2}, \tag{5}$$

where $\Delta m = 1(2)$ is the change in spin quantum number in the SQ (DQ) basis and $\delta_\mathrm{N} = \gamma_\mathrm{N}/2\pi$ is the Lorentzian linewidth (half width at half maximum) of the nitrogen spin resonances measured through DEER ESR [Fig. 1(d)]. Although we find that NV and nitrogen spins have comparable T_2^* ($\gamma_{\mathrm{NV\text{-}N}} \approx \gamma_\mathrm{N}$, see Supplemental Material Sec. XI [28]), the effective linewidth δ_N relevant for bath driving is increased due to imperfect overlap of the nitrogen spin resonances caused by a small misalignment angle of the applied bias magnetic field.

Using the NV-N dipolar estimate for sample B, $\gamma_{\mathrm{NV\text{-}N}} \approx 2\pi \times 7$ kHz, $\delta_\mathrm{N} \approx 80$ kHz extracted from DEER measurements (Supplemental Material Sec. XI [28]), and a saturation value of $T^*_{2,\mathrm{other}} \approx 27$ μs, we combine Eqs. (4) and (5) and plot the calculated T_2^* as a function of Ω_N in Fig. 4(a) (black, dashed line). The good agreement between the model and our data in the DQ basis suggests that Eqs. (4) and (5) capture the dependence of T_2^* on drive field magnitude (i.e., Rabi frequency). Alternatively, we fit the model to the DQ data (red, solid line) and extract $\gamma^{\mathrm{fit}}_{\mathrm{NV\text{-}N}} = 2\pi \times 9.3(2)$ kHz and $\delta^{\mathrm{fit}}_\mathrm{N} = 60(3)$ kHz, in reasonable agreement with our estimated parameters. In summary, the results from sample B show that the combination of spin-bath driving and sensing in the DQ basis suppresses inhomogeneous NV ensemble dephasing due to both interactions with the nitrogen spin bath and strain gradients. Similar to sample A, further enhancement in T_2^* could be achieved with improved isotopic purity, as well as reduced magnetic gradients due to the applied magnetic bias field.

C. Dipolar-dominated dephasing (Sample C: High nitrogen density regime)

Spin-bath driving results for sample C ([N] = 10 ppm, ^{15}N) are shown in Fig. 4(b). At this high nitrogen density, interactions with the nitrogen bath dominate NV spin ensemble dephasing, and $T^*_{2,\mathrm{SQ}}$ and $T^*_{2,\mathrm{DQ}}$ both exhibit a clear dependence on spin-bath drive strength Ω_N. With no drive ($\Omega_\mathrm{N} = 0$), we measured $T^*_{2,\mathrm{DQ}} \approx T^*_{2,\mathrm{SQ}}/2$, in agreement with dephasing dominated by a paramagnetic spin environment and the twice higher precession rate in the DQ basis [30,31,52]. Note that this result is in contrast to the observed DQ basis enhancement of T_2^* at lower nitrogen density for samples A and B (Figs. 2 and 3). We also find that T_2^* in sample C increases more rapidly as a function of spin-bath drive amplitude in the DQ basis than in the SQ basis, such that $T^*_{2,\mathrm{DQ}}$ surpasses $T^*_{2,\mathrm{SQ}}$ with sufficient spin-bath drive strength. We attribute the T_2^* limit in the SQ basis ($\simeq$1.8 μs) to strain inhomogeneities in this sample, whereas the longest observed T_2^* in the DQ basis ($\simeq$3.4 μs) is in agreement with dephasing due to the 0.05% ^{13}C and 0.5 ppm residual ^{14}N spin impurities. The latter were incorporated during growth of this ^{15}N sample (see Supplemental Material Table S5 [28]).

In Fig. 4(c), we plot $T^*_{2,\mathrm{NV\text{-}N}} \equiv 2 \times T^*_{2,\mathrm{DQ}}$ versus sample nitrogen concentration [N] to account for the twice faster dephasing of the DQ coherence. To improve the range of [N] coverage, we include DQ data for additional diamonds, samples D ([N] = 3 ppm) and E ([N] = 48 ppm). To our knowledge, the dependence of the NV spin ensemble dephasing time on [N] has not previously been experimentally reported. Fitting the data to the function $1/T^*_{2,\mathrm{NV\text{-}N}} = A_{\mathrm{NV\text{-}N}} \cdot [\mathrm{N}]$ (red shaded region), we find the characteristic NV-N interaction strength for NV ensembles to be $A_{\mathrm{NV\text{-}N}} = 2\pi \times 16.6(2.6)$ kHz/ppm [$1/A_{\mathrm{NV\text{-}N}} = 9.6(1.8)\mu\mathrm{s} \cdot \mathrm{ppm}$] in the SQ sub-basis. This value is about 1.8× larger than the dipolar-estimate $\gamma_{e-e} = 2\pi \times 9.1$ kHz/ppm (black dashed-dotted line), which is used above in estimates of NV dephasing due to the nitrogen spin bath. We also performed numerical spin-bath simulations for the NV-N spin system and determined the second moment of the dipolar-broadened single NV ESR linewidth [50] [Chaps. III and IV]. By simulating 10^4 random spin-bath configurations, we extract the ensemble-averaged dephasing time from the distribution of the single NV linewidths [51]. The results of this simulation (black dashed line) are in excellent agreement with the experiment and confirm the validity of our obtained

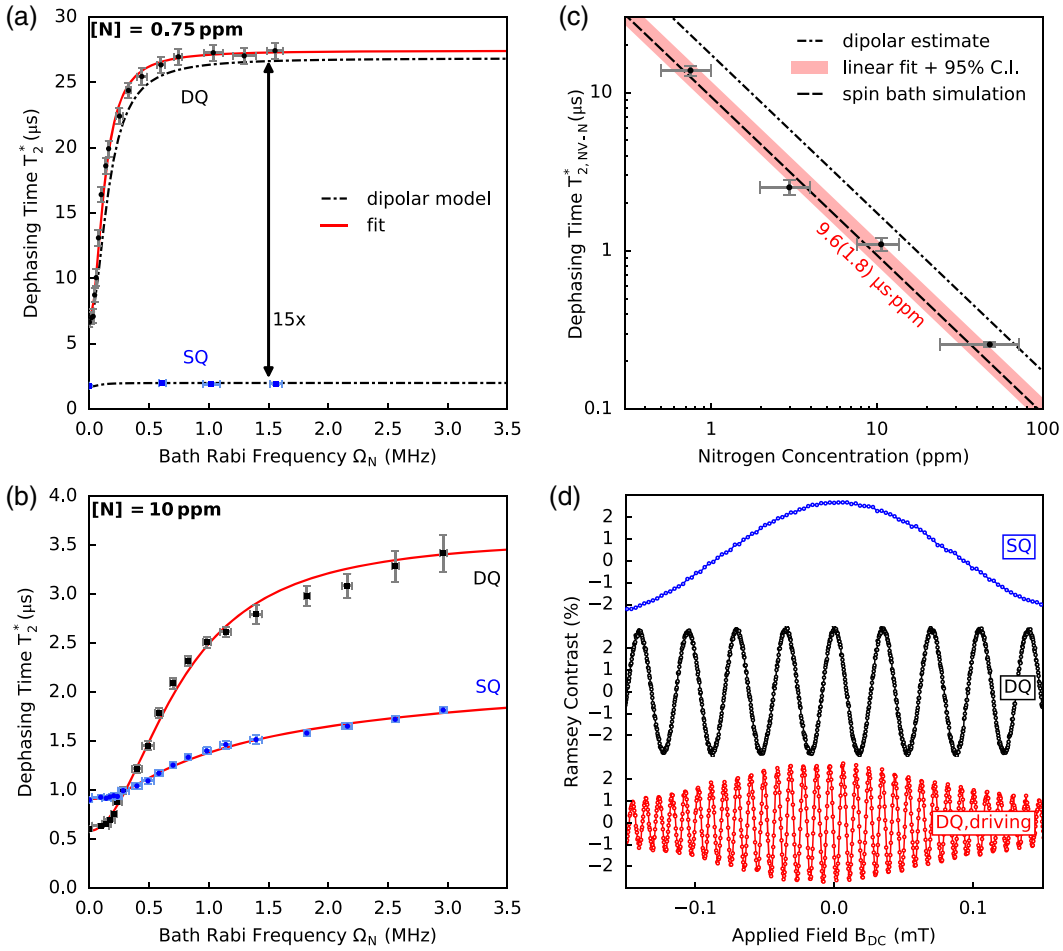

FIG. 4. Application of quantum control techniques to extend NV spin ensemble dephasing time (T_2^*) and increase dc magnetic-field sensitivity. (a) Ramsey measurements of T_2^* in the single quantum (SQ, blue) and double quantum (DQ, black) bases for different spin-bath drive strengths (Rabi frequencies) for sample B ($[\mathrm{N}] = 0.75$ ppm) at $B_0 = 8.5$ mT. The black dashed-dotted line is calculated from a model of NV spins that are dipolar coupled to a multicomponent spin bath [Eq. (4)]. The red solid line is a fit of the model to the T_2^* data (see main text for details). (b) Same as (a) but for sample C ($[\mathrm{N}] = 10$ ppm) and $B_0 = 10.3$ mT. (c) Measured $T^*_{2,\mathrm{NV\text{-}N}} \equiv 2 \times T^*_{2,\mathrm{DQ}}$ as a function of nitrogen concentration for samples B, C, D, E. Samples were selected to have a predominately electronic nitrogen (P1) spin bath using DEER ESR measurements. The black dashed-dotted line is the dipolar-interaction-estimated dependence of T_2^* on nitrogen concentration (Supplemental Material Sec. V [28]). We fit the data using an orthogonal-distance-regression routine to account for the uncertainties in [N] and T_2^*. A fit to the form $1/T_2^* = A_{\mathrm{NV\text{-}N}}[\mathrm{N}]$ yields $A_{\mathrm{N\text{-}NV}} = 2\pi \times 16.6(2.6)$ kHz/ppm $[1/A_{\mathrm{NV\text{-}N}} = 9.6(1.8)\ \mu\mathrm{s} \cdot \mathrm{ppm}]$. The red shaded region indicates the 95% standard error of the fit value for $A_{\mathrm{NV\text{-}N}}$. The black dashed line is the expected scaling extracted from numerical simulations using a second-moment analysis of the NV ensemble ESR linewidth (see text for details). (d) Measured Ramsey dc magnetometry signal $S \propto C \sin[\phi(\tau)]$ for sample B, in the SQ and DQ bases, as well as the DQ sub-basis with spin-bath drive (see main text for details). There is a 36× faster oscillation in the DQ sub-basis with spin-bath drive compared to SQ with no drive. This greatly enhanced dc magnetic-field sensitivity is a direct result of the extended T_2^*, with the sensitivity enhancement given by $2 \times \sqrt{\tau_{\mathrm{DQ+Drive}}/\tau_{\mathrm{SQ}}}$ at equal contrast. The slight decrease in observed contrast in the DQ + drive case for $|B_{\mathrm{dc}}| > 0.05$ mT is a result of changes in the Zeeman resonance frequencies of the nitrogen spins due to the applied test field B_{dc}, which was not corrected for in these measurements.

scaling for $T^*_{2,\mathrm{NV\text{-}N}}(\mathrm{N})$. Additional details of the simulation are provided in Ref. [53].

D. Ramsey dc magnetic-field sensing

We demonstrated that combining the two quantum control techniques can greatly improve the sensitivity of Ramsey dc magnetometry. Figure 4(d) compares the accumulated phase for SQ, DQ, and DQ plus spin-bath drive measurements of a tunable static magnetic field of amplitude B_{dc}, for sample B. Sweeping B_{dc} leads to a characteristic observed oscillation of the Ramsey signal $S \propto C \sin(\phi)$, where $C = C_0 \exp[-(\tau/T_2^*)^p]$ is the measurement contrast and $\phi = \Delta m \times \gamma_{\mathrm{NV}} B_{\mathrm{dc}} \tau$ is the accumulated phase during the free

precession interval $\tau \approx T_2^*$. Choosing $\tau_{SQ} = 1.308\ \mu$s and $\tau_{DQ+Drive} = 23.99\ \mu$s (see Supplemental Material Sec. XII [28]), we find a $36.3(1.9)\times$ faster oscillation period (at equal measurement contrast) when DQ and spin-bath driving are both employed, compared to a SQ measurement. This enhancement in phase accumulation, and hence dc magnetic-field sensitivity, agrees well with the expected improvement ($2 \times \tau_{DQ+Drive}/\tau_{SQ} = 36.7$).

III. DISCUSSION

Our results (i) characterize the dominant spin dephasing mechanisms for NV ensembles in bulk diamond (strain and interactions with the paramagnetic spin bath) and (ii) demonstrate that the combination of DQ magnetometry and spin-bath driving can greatly extend the NV spin ensemble T_2^*. For example, in sample B we find that these quantum control techniques, when combined, provide a $16.2\times$ improvement in T_2^*. Operation in the DQ basis protects against common-mode inhomogeneities and enables an extension of T_2^* for samples with $[\mathrm{N}] \lesssim 1$ ppm. In such samples, strain inhomogeneities are found to be the main causes of NV spin ensemble dephasing. In samples with higher N concentration ($[\mathrm{N}] \gtrsim 1$ ppm), spin-bath driving in combination with DQ sensing provides an increase of the NV ensemble T_2^* by decoupling paramagnetic nitrogen and other electronic dark spins from the NV spins. Our results suggest that quantum control techniques may allow the NV ensemble T_2^* to approach the bare Hahn echo coherence time T_2. Note that spin-bath driving may also be used to enhance the NV ensemble T_2 in Hahn echo, dynamical decoupling [25,26], and spectral decomposition experimental protocols [54].

Furthermore, we showed that the combination of DQ magnetometry and spin-bath driving allows improved dc Ramsey magnetic-field sensing. The relative enhancement in photon-shot-noise-limited sensitivity (neglecting experimental overhead time) is quantified by $2 \times \sqrt{\zeta}$, where the factor of two accounts for the enhanced gyromagnetic ratio in the DQ basis and $\zeta \equiv T_{2,DQ}^*/T_{2,SQ}^*$ is the ratio of maximally achieved T_2^* in the DQ basis (with spin-bath drive when advantageous) and nondriven T_2^* in the SQ basis. For samples A, B, and C, we calculate $2 \times \sqrt{\zeta} = 5.2\times$, $8.1\times$, and $3.9\times$, respectively, using our experimental values. In practice, increasing T_2^* also decreases the fractional overhead time associated with NV optical initialization and readout, resulting in even greater dc magnetic-field sensitivity improvements and an approximately linear sensitivity enhancement with ζ (see Supplemental Material Sec. XII [28]). We expect that these quantum control techniques will remain effective when integrated with other approaches to optimize NV ensemble magnetic-field sensitivity, such as high laser power and good N-to-NV conversion efficiency. In particular, conversion efficiencies of 1–30% have been reported for NV ensemble measurements [13,21,23,55], such that the nitrogen spin bath continues to be a relevant spin dephasing mechanism.

There are multiple avenues for further improvement in NV ensemble T_2^* and dc magnetic-field sensitivity, beyond the gains demonstrated in this work. First, the ^{13}C limitation to T_2^*, observed for all samples, can be mitigated via improved isotopic purity ($[^{12}\mathrm{C}] > 99.99\%$) or possibly through driving of the nuclear spin bath [56]. Second, more efficient rf delivery will enable faster spin-bath driving (higher Rabi drive frequency Ω_N), which will be critical for decoupling denser nitrogen baths and thereby extending $T_2^* \propto \Omega_N^2/\delta_N^2 \propto \Omega_N^2/[\mathrm{N}]^2$ [see Eq. (5)]. Third, short NV ensemble T_2^* times have so far prevented effective utilization of more exotic readout techniques, e.g., involving quantum logic [57–59] or spin-to-charge conversion [60,61]. Such methods offer greatly improved NV spin-state readout fidelity but introduce substantial overhead time, typically requiring tens to hundreds of microseconds per readout operation. The NV spin ensemble dephasing times demonstrated in this work ($T_2^* \gtrsim 20\ \mu$s) may allow effective application of these readout schemes, which only offer sensitivity improvements when the sequence sensing time (set by T_2^* for dc sensing) is comparable to the added overhead time. We note that the NV ensemble T_2^* values obtained in this work are the longest for any electronic solid-state spin system at room temperature (see comparison in Fig. S2) suggesting that state-of-the-art dc magnetic-field sensitivity [13,62] may be increased to approximately $100\ \mathrm{fT}/\sqrt{\mathrm{Hz}}$ for optimized NV ensembles in a diamond sensing volume $\sim(100\ \mu\mathrm{m})^3$ (see discussion on NV ensemble dc magnetic-field sensitivity optimization in Ref. [13]). In conclusion, DQ magnetometry in combination with spin-bath driving allows for an order-of-magnitude increase in the NV ensemble T_2^* in diamond, providing a clear path to ultrahigh-sensitivity dc magnetometry with NV ensemble coherence times approaching T_2.

ACKNOWLEDGMENTS

We thank David Le Sage for his initial contributions to this project. We thank Joonhee Choi, Soonwon Choi, and Renate Landig for fruitful discussions. This material is based upon work supported by, or in part by, the United States Army Research Laboratory and the United States Army Research Office under Grant No. W911NF-15-1-0548; the National Science Foundation Electronics, Photonics and Magnetic Devices (EPMD), Physics of Living Systems (PoLS), and Integrated NSF Support Promoting Interdisciplinary Research and Education (INSPIRE) programs under Grants No. ECCS-1408075, No. PHY-1504610, and No. EAR-1647504, respectively; and Lockheed Martin under Contract No. A32198. This work was performed in part at the Center for Nanoscale Systems (CNS), a member of the National Nanotechnology Coordinated Infrastructure Network (NNCI), which is

supported by the National Science Foundation under NSF Grant No. 1541959. CNS is part of Harvard University. P. K. acknowledges support from the Intelligence Community Postdoctoral Research Fellowship Program. J. M. S. was supported by a Fannie and John Hertz Foundation Graduate Fellowship and a NSF Graduate Research Fellowship under Grant No. 1122374.

E. B., C. A. H., J. M. S., M. J. T., J. F. B., and R. L. W. conceived the experiments; C. A. H. and E. B. conducted the experiments and analyzed the results. P. K. provided the strain analysis. E. B. and S. S. provided the spin-bath simulation. All authors contributed to and reviewed the manuscript. R. L. W. supervised the work.

[1] P. V. Klimov, A. L. Falk, D. J. Christle, V. V. Dobrovitski, and D. D. Awschalom, *Quantum Entanglement at Ambient Conditions in a Macroscopic Solid-State Spin Ensemble*, Sci. Adv. **1**, e1501015 (2015).

[2] M. Widmann, S.-Y. Lee, T. Rendler, N. T. Son, H. Fedder, S. Paik, L.-P. Yang, N. Zhao, S. Yang, I. Booker, A. Denisenko, M. Jamali, S. Ali Momenzadeh, I. Gerhardt, T. Ohshima, A. Gali, E. Janzén, and J. Wrachtrup, *Coherent Control of Single Spins in Silicon Carbide at Room Temperature*, Nat. Mater. **14**, 164 (2015).

[3] F. J. Heremans, C. G. Yale, and D. D. Awschalom, *Control of Spin Defects in Wide-Bandgap Semiconductors for Quantum Technologies*, Proc. IEEE **104**, 2009 (2016).

[4] W. F. Koehl, B. Diler, S. J. Whiteley, A. Bourassa, N. T. Son, E. Janzén, and D. D. Awschalom, *Resonant Optical Spectroscopy and Coherent Control of* Cr4 + Spin *Ensembles in SiC and GaN*, Phys. Rev. B **95**, 035207 (2017).

[5] S. A. Tarasenko, A. V. Poshakinskiy, D. Simin, V. A. Soltamov, E. N. Mokhov, P. G. Baranov, V. Dyakonov, and G. V. Astakhov, *Spin and Optical Properties of Silicon Vacancies in Silicon Carbide—A Review*, Phys. Status Solidi (b) **255**, 1700258 (2018).

[6] E. Abe, A. M. Tyryshkin, S. Tojo, J. J. L. Morton, W. M. Witzel, A. Fujimoto, J. W. Ager, E. E. Haller, J. Isoya, S. A. Lyon, M. L. W. Thewalt, and K. M. Itoh, *Electron Spin Coherence of Phosphorus Donors in Silicon: Effect of Environmental Nuclei*, Phys. Rev. B **82**, 121201 (2010).

[7] A. M. Tyryshkin, S. Tojo, J. J. L. Morton, H. Riemann, N. V. Abrosimov, P. Becker, H.-J. Pohl, T. Schenkel, M. L. W. Thewalt, K. M. Itoh, and S. A. Lyon, *Electron Spin Coherence Exceeding Seconds in High-Purity Silicon*, Nat. Mater. **11**, 143 (2012).

[8] C. Hepp, T. Müller, V. Waselowski, J. N. Becker, B. Pingault, H. Sternschulte, D. Steinmüller-Nethl, A. Gali, J. R. Maze, M. Atatüre, and C. Becher, *Electronic Structure of the Silicon Vacancy Color Center in Diamond*, Phys. Rev. Lett. **112**, 036405 (2014).

[9] B. C. Rose, D. Huang, Z.-h. Zhang, A. M. Tyryshkin, S. Sangtawesin, S. Srinivasan, L. Loudin, M. L. Markham, A. M. Edmonds, D. J. Twitchen, S. A. Lyon, and N. P. de Leon, *Observation of an Environmentally Insensitive Solid State Spin Defect in Diamond* (to be published).

[10] M. W. Doherty, N. B. Manson, P. Delaney, F. Jelezko, J. Wrachtrup, and L. C. L. Hollenberg, *The Nitrogen-Vacancy Colour Centre in Diamond*, Phys. Rep. **528**, 1 (2013).

[11] G. Balasubramanian, P. Neumann, D. Twitchen, M. Markham, R. Kolesov, N. Mizuochi, J. Isoya, J. Achard, J. Beck, J. Tissler, V. Jacques, P. R. Hemmer, F. Jelezko, and J. Wrachtrup, *Ultralong Spin Coherence Time in Isotopically Engineered Diamond*, Nat. Mater. **8**, 383 (2009).

[12] P. L. Stanwix, L. M. Pham, J. R. Maze, D. Le Sage, T. K. Yeung, P. Cappellaro, P. R. Hemmer, A. Yacoby, M. D. Lukin, and R. L. Walsworth, *Coherence of Nitrogen-Vacancy Electronic Spin Ensembles in Diamond*, Phys. Rev. B **82**, 201201 (2010).

[13] J. F. Barry, M. J. Turner, J. M. Schloss, D. R. Glenn, Y. Song, M. D. Lukin, H. Park, and R. L. Walsworth, *Optical Magnetic Detection of Single-Neuron Action Potentials Using Quantum Defects in Diamond*, Proc. Natl. Acad. Sci. U.S.A. **113**, 14133 (2016).

[14] D. R. Glenn, D. B. Bucher, J. Lee, M. D. Lukin, H. Park, and R. L. Walsworth, *High-Resolution Magnetic Resonance Spectroscopy Using a Solid-State Spin Sensor*, Nature (London) **555**, 351 (2018).

[15] D. Le Sage, K. Arai, D. R. Glenn, S. J. DeVience, L. M. Pham, L. Rahn-Lee, M. D. Lukin, A. Yacoby, A. Komeili, and R. L. Walsworth, *Optical Magnetic Imaging of Living Cells*, Nature (London) **496**, 486 (2013).

[16] D. R. Glenn, K. Lee, H. Park, R. Weissleder, A. Yacoby, M. D. Lukin, H. Lee, R. L. Walsworth, and C. B. Connolly, *Single-Cell Magnetic Imaging Using a Quantum Diamond Microscope*, Nat. Methods **12**, 736 (2015).

[17] L. Shao, R. Liu, M. Zhang, A. V. Shneidman, X. Audier, M. Markham, H. Dhillon, D. J. Twitchen, Y.-F. Xiao, and M. Lončar, *Wide-Field Optical Microscopy of Microwave Fields Using Nitrogen-Vacancy Centers in Diamonds*, Adv. Opt. Mater., **4** 1075 (2016).

[18] J.-P. Tetienne, N. Dontschuk, D. A. Broadway, A. Stacey, D. A. Simpson, and L. C. L. Hollenberg, *Quantum Imaging of Current Flow in Graphene*, Sci. Adv. **3**, e1602429 (2017).

[19] D. R. Glenn, R. R. Fu, P. Kehayias, D. Le Sage, E. A. Lima, B. P. Weiss, and R. L. Walsworth, *Micrometer-Scale Magnetic Imaging of Geological Samples Using a Quantum Diamond Microscope*, Geochem. Geophys. Geosyst. **18**, 3254 (2017).

[20] R. R. Fu, B. P. Weiss, E. A. Lima, P. Kehayias, J. F. D. F. Araujo, D. R. Glenn, J. Gelb, J. F. Einsle, A. M. Bauer, R. J. Harrison, G. A. H. Ali, and R. L. Walsworth, *Evaluating the Paleomagnetic Potential of Single Zircon Crystals Using the Bishop Tuff*, Earth Planet. Sci. Lett. **458**, 1 (2017).

[21] V. M. Acosta, E. Bauch, M. P. Ledbetter, A. Waxman, L.-S. Bouchard, and D. Budker, *Temperature Dependence of the Nitrogen-Vacancy Magnetic Resonance in Diamond*, Phys. Rev. Lett. **104**, 070801 (2010).

[22] Y. Kubo, C. Grezes, A. Dewes, T. Umeda, J. Isoya, H. Sumiya, N. Morishita, H. Abe, S. Onoda, T. Ohshima, V. Jacques, A. Dréau, J. F. Roch, I. Diniz, A. Auffeves, D. Vion, D. Esteve, and P. Bertet, *Hybrid Quantum Circuit with a Superconducting Qubit Coupled to a Spin Ensemble*, Phys. Rev. Lett. **107**, 220501 (2011).

[23] C. Grezes, B. Julsgaard, Y. Kubo, W. L. Ma, M. Stern, A. Bienfait, K. Nakamura, J. Isoya, S. Onoda, T. Ohshima, V.

Jacques, D. Vion, D. Esteve, R. B. Liu, K. Mølmer, and P. Bertet, *Storage and Retrieval of Microwave Fields at the Single-Photon Level in a Spin Ensemble*, Phys. Rev. A **92**, 020301 (2015).

[24] J. Choi, S. Choi, G. Kucsko, P. C. Maurer, B. J. Shields, H. Sumiya, S. Onoda, J. Isoya, E. Demler, F. Jelezko, N. Y. Yao, and M. D. Lukin, *Depolarization Dynamics in a Strongly Interacting Solid-State Spin Ensemble*, Phys. Rev. Lett. **118**, 093601 (2017).

[25] G. de Lange, Z. H. Wang, D. Riste, V. V. Dobrovitski, and R. Hanson, *Universal Dynamical Decoupling of a Single Solid-State Spin from a Spin Bath*, Science **330**, 60 (2010).

[26] L. M. Pham, N. Bar-Gill, C. Belthangady, D. Le Sage, P. Cappellaro, M. D. Lukin, A. Yacoby, and R. L. Walsworth, *Enhanced Solid-State Multispin Metrology Using Dynamical Decoupling*, Phys. Rev. B **86**, 045214 (2012).

[27] N. Bar-Gill, L. M. Pham, A. Jarmola, D. Budker, and R. L. Walsworth, *Solid-State Electronic Spin Coherence Time Approaching One Second*, Nat. Commun. **4**, 1743 (2013).

[28] See Supplemental Material at http://link.aps.org/supplemental/10.1103/PhysRevX.8.031025 for further references and detailed information.

[29] P. C. Maurer, G. Kucsko, C. Latta, L. Jiang, N. Y. Yao, S. D. Bennett, F. Pastawski, D. Hunger, N. Chisholm, M. Markham, D. J. Twitchen, J. I. Cirac, and M. D. Lukin, *Room-Temperature Quantum Bit Memory Exceeding One Second*, Science **336**, 1283 (2012).

[30] K. Fang, V. M. Acosta, C. Santori, Z. Huang, K. M. Itoh, H. Watanabe, S. Shikata, and R. G. Beausoleil, *High-Sensitivity Magnetometry Based on Quantum Beats in Diamond Nitrogen-Vacancy Centers*, Phys. Rev. Lett. **110**, 130802 (2013).

[31] H. J. Mamin, M. H. Sherwood, M. Kim, C. T. Rettner, K. Ohno, D. D. Awschalom, and D. Rugar, *Multipulse Double-Quantum Magnetometry with Near-Surface Nitrogen-Vacancy Centers*, Phys. Rev. Lett. **113**, 030803 (2014).

[32] G. de Lange, T. van der Sar, M. Blok, Z.-H. Wang, V. Dobrovitski, and R. Hanson, *Controlling the Quantum Dynamics of a Mesoscopic Spin Bath in Diamond*, Sci. Rep. **2**, 382 (2012).

[33] H. S. Knowles, D. M. Kara, and M. Atatüre, *Observing Bulk Diamond Spin Coherence in High-Purity Nanodiamonds*, Nat. Mater. **13**, 21 (2014).

[34] W. V. Smith, P. P. Sorokin, I. L. Gelles, and G. J. Lasher, *Electron-Spin Resonance of Nitrogen Donors in Diamond*, Phys. Rev. **115**, 1546 (1959).

[35] R. J. Cook and D. H. Whiffen, *Electron Nuclear Double Resonance Study of a Nitrogen Centre in Diamond*, Proc. R. Soc. A **295**, 99 (1966).

[36] J. H. N. Loubser and J. A. van Wyk, *Electron Spin Resonance in the Study of Diamond*, Rep. Prog. Phys. **41**, 1201 (1978).

[37] N. Mizuochi, P. Neumann, F. Rempp, J. Beck, V. Jacques, P. Siyushev, K. Nakamura, D. J. Twitchen, H. Watanabe, S. Yamasaki, F. Jelezko, and J. Wrachtrup, *Coherence of Single Spins Coupled to a Nuclear Spin Bath of Varying Density*, Phys. Rev. B **80**, 041201 (2009).

[38] A. Dréau, J. R. Maze, M. Lesik, J. F. Roch, and V. Jacques, *High-Resolution Spectroscopy of Single NV Defects Coupled with Nearby 13C Nuclear Spins in Diamond*, Phys. Rev. B **85**, 134107 (2012).

[39] P. Jamonneau, M. Lesik, J. P. Tetienne, I. Alvizu, L. Mayer, A. Dréau, S. Kosen, J. F. Roch, S. Pezzagna, J. Meijer, T. Teraji, Y. Kubo, P. Bertet, J. R. Maze, and V. Jacques, *Competition between Electric Field and Magnetic Field Noise in the Decoherence of a Single Spin in Diamond*, Phys. Rev. B **93**, 024305 (2016).

[40] M. E. Trusheim and D. Englund, *Wide-Field Strain Imaging with Preferentially Aligned Nitrogen-Vacancy Centers in Polycrystalline Diamond*, New J. Phys. **18**, 123023 (2016).

[41] M. P. Gaukroger, P. M. Martineau, M. J. Crowder, I. Friel, S. D. Williams, and D. J. Twitchen, *X-ray Topography Studies of Dislocations in Single Crystal CVD Diamond*, Diam. Relat. Mater. **17**, 262 (2008).

[42] L. T. M. Hoa, T. Ouisse, D. Chaussende, M. Naamoun, A. Tallaire, and J. Achard, *Birefringence Microscopy of Unit Dislocations in Diamond*, Cryst. Growth Des. **14**, 5761 (2014).

[43] M. S. J. Barson, P. Peddibhotla, P. Ovartchaiyapong, K. Ganesan, R. L. Taylor, M. Gebert, Z. Mielens, B. Koslowski, D. A. Simpson, L. P. McGuinness, J. McCallum, S. Prawer, S. Onoda, T. Ohshima, A. C. B. Jayich, F. Jelezko, N. B. Manson, and M. W. Doherty, *Nanomechanical Sensing Using Spins in Diamond*, Nano Lett. **17**, 1496 (2017).

[44] D. M. Toyli, C. F. de las Casas, D. J. Christle, V. V. Dobrovitski, and D. D. Awschalom, *Fluorescence Thermometry Enhanced by the Quantum Coherence of Single Spins in Diamond*, Proc. Natl. Acad. Sci. U.S.A. **110**, 8417 (2013).

[45] P. Keller, *Basic Principles of Magnetic Resonance*, Springer Series in Solid-State Sciences Vol. 1 (Springer Berlin Heidelberg, Berlin, Heidelberg, 2010), pp. 1–30.

[46] C. A. J. Ammerlaan and E. A. Burgemeister, *Reorientation of Nitrogen in Type-Ib Diamond by Thermal Excitation and Tunneling*, Phys. Rev. Lett. **47**, 954 (1981).

[47] G. Davies, *Dynamic Jahn-Teller Distortions at Trigonal Optical Centres in Diamond*, J. Phys. C **12**, 2551 (1979).

[48] G. Davies, *The Jahn-Teller Effect and Vibronic Coupling at Deep Levels in Diamond*, Rep. Prog. Phys. **44**, 787 (1981).

[49] T. Yamamoto, T. Umeda, K. Watanabe, S. Onoda, M. L. Markham, D. J. Twitchen, B. Naydenov, L. P. McGuinness, T. Teraji, S. Koizumi, F. Dolde, H. Fedder, J. Honert, J. Wrachtrup, T. Ohshima, F. Jelezko, and J. Isoya, *Extending Spin Coherence Times of Diamond Qubits by High-Temperature Annealing*, Phys. Rev. B **88**, 075206 (2013).

[50] A. Abragam, *The Principles of Nuclear Magnetism* (Clarendon Press, Oxford, 1983), p. 599.

[51] V. V. Dobrovitski, A. E. Feiguin, D. D. Awschalom, and R. Hanson, *Decoherence Dynamics of a Single Spin versus Spin Ensemble*, Phys. Rev. B **77**, 245212 (2008).

[52] E. R. MacQuarrie, T. A. Gosavi, A. M. Moehle, N. R. Jungwirth, S. A. Bhave, and G. D. Fuchs, *Coherent Control of a Nitrogen-Vacancy Center Spin Ensemble with a Diamond Mechanical Resonator*, Optica **2**, 233 (2015).

[53] E. Bauch, P. Jungyun, C. Hart, S. Singh, J. M. Schloss, M. J. Turner, J. F. Barry, L. Pham, N. Bar-Gill, S. F. Yelin, and R. Walsworth, *Quantum Coherence of NV Center Solid-State Spins in Diamond* (to be published).

[54] N. Bar-Gill, L. M. Pham, C. Belthangady, D. Le Sage, P. Cappellaro, J. R. Maze, M. D. Lukin, A. Yacoby, and R. Walsworth, *Suppression of Spin-Bath Dynamics for*

Improved Coherence of Multi-Spin-Qubit Systems, Nat. Commun. **3**, 858 (2012).

[55] T. Wolf, P. Neumann, K. Nakamura, H. Sumiya, T. Ohshima, J. Isoya, and J. Wrachtrup, *Subpicotesla Diamond Magnetometry*, Phys. Rev. X **5**, 041001 (2015).

[56] P. London, J. Scheuer, J. M. Cai, I. Schwarz, A. Retzker, M. B. Plenio, M. Katagiri, T. Teraji, S. Koizumi, J. Isoya, R. Fischer, L. P. McGuinness, B. Naydenov, and F. Jelezko, *Detecting and Polarizing Nuclear Spins with Double Resonance on a Single Electron Spin*, Phys. Rev. Lett. **111**, 067601 (2013).

[57] L. Jiang, J. S. Hodges, J. R. Maze, P. Maurer, J. M. Taylor, D. G. Cory, P. R. Hemmer, R. L. Walsworth, A. Yacoby, A. S. Zibrov, and M. D. Lukin, *Repetitive Readout of a Single Electronic Spin via Quantum Logic with Nuclear Spin Ancillae*, Science **326**, 267 (2009).

[58] P. Neumann, J. Beck, M. Steiner, F. Rempp, H. Fedder, P. R. Hemmer, J. Wrachtrup, and F. Jelezko, *Single-Shot Readout of a Single Nuclear Spin*, Science **329**, 542 (2010).

[59] I. Lovchinsky, A. O. Sushkov, E. Urbach, N. P. de Leon, S. Choi, K. De Greve, R. Evans, R. Gertner, E. Bersin, C. Muller, L. McGuinness, F. Jelezko, R. L. Walsworth, H. Park, and M. D. Lukin, *Nuclear Magnetic Resonance Detection and Spectroscopy of Single Proteins Using Quantum Logic*, Science **351**, 836 (2016).

[60] B. J. Shields, Q. P. Unterreithmeier, N. P. de Leon, H. Park, and M. D. Lukin, *Efficient Readout of a Single Spin State in Diamond via Spin-to-Charge Conversion*, Phys. Rev. Lett. **114**, 136402 (2015).

[61] J.-C. Jaskula, B. J. Shields, E. Bauch, M. D. Lukin, A. S. Trifonov, and R. L. Walsworth, *Improved Quantum Sensing with a Single Solid-State Spin via Spin-to-Charge Conversion*, arXiv:1711.02023.

[62] G. Chatzidrosos, A. Wickenbrock, L. Bougas, N. Leefer, T. Wu, K. Jensen, Y. Dumeige, and D. Budker, *Miniature Cavity-Enhanced Diamond Magnetometer*, Phys. Rev. Applied **8**, 044019 (2017).